CHAPTER 3

Overview to the Theoretical Studies on Polyoxometalates

During the last ten years, a few theoretical groups settled the basis for a new viewpoint in the understanding of polyoxometalates' characteristics. The aim of computational chemistry applied to such molecules is to give explanations to partially unknown phenomena, as well as general guidelines of behaviour. Computational chemistry has proven to be a powerful tool to the analysis of chemical systems. Various techniques have been developed and successfully applied to study systems ranging from small molecules to extended solids. In this chapter we summarise the quantum chemistry studies carried out by several groups before and during the realisation of this thesis. Here, we discuss in brief the most significant results obtained by means of the *ab initio* and the density-functional theory formulations. The acceptance of these works amongst the experimental community is growing and, for the time being, the information obtained by means of computational and *traditional* chemistry complements each other.

3.1. Introduction

Computational Transition Metal Chemistry has reached its maturity, basically due to the widespread acceptance of methods based on the density functional theory (DFT). In the 1970's, the *ab initio* Hartree–Fock (HF) approximation provided a reasonable starting point for studying small- to medium-sized organic molecules and for understanding reaction mechanisms involving small organic molecules. Later, Møller–Plesset perturbation theory, configuration interaction, coupled cluster theory and other methods provided a more quantitative description. For transition metals, the error in HF methods, the so-called *correlation energy*, is generally too large. Part of the correlation energy can be introduced using DFT methods. These give reliable structures and bonding energies with only moderate computational effort. Many organometallic and polynuclear structures have been described using DFT.[1] However, the number of high-level computational studies on POMs can be considered still quite low. A combination of three factors —the large size of polyoxoanions, the presence of transition metal ions and the high negative charge— produce, in practice, important computational limitations. In the last ten years, a few groups have been especially active and have made important progress in describing and rationalising the electronic and magnetic properties of POMs. The first studies by Marc Bénard were performed at the HF level. Later investigations preferentially used density functional methods, as implemented in the ADF set of programs.[2] Even though, some extended-Hückel calculations were carried out applied to heteropolyanions, as well.[3-5] In this chapter we review the most significant theoretical studies in the field of POMs. To do this, we stress more on the results achieved and less on the methods used. This chapter is based on a recently published review performed by our group in the context of the present thesis.[6]

This chapter is divided into two main parts. In section 3.2 we summarise works released previous to the beginning of the present PhD. work in 1999. Section 3.3 contains publications dating from that year to present except those published by the author of this thesis, which are discussed in chapters of Part II.

3.2. Previous Theoretical Studies

Relative basicity of the oxo sites in $V_{10}O_{28}$

Heteropoly acids are considered to be significantly stronger than typical inorganic acids such as H_2SO_4, HNO_3, HCl, etc. The negative charge of HPAs, which are larger than inorganic acids, is delocalised among a large number of oxygen sites, so the electrostatic interactions between the proton and the anion are weaker. In general, heteropolytungstates are more acidic than molybdates, whereas the effect of the heteroatom is less important. The order of acid strength for some heteropoly acids is $H_3PW_{12}O_{40}$ > $H_4SiW_{12}O_{40}$ > $H_4GeW_{12}O_{40}$ > $H_6P_2W_{16}O_{62}$ and $H_3PW_{12}O_{40}$ > $H_3PMo_{12}O_{40}$. Davis and co-workers[7] evaluated the acidity of $H_3PW_{12}O_{40}$ > $H_3PMo_{12}O_{40}$ by calculating the proton affinity from the process $H_3PM_{12}O_{40} \rightarrow H_2PM_{12}O_{40}^- + H^+$. The protons in $H_3PM_{12}O_{40}$ were placed at bridging positions far away from one another. The cluster energies were computed after the complete optimisation of the diprotonated and triprotonated species. The value of 1126 kJ mol^{-1} for the third bridging site in the phosphomolybdate was 38 kJ mol^{-1} larger than the proton affinity found for the tungstate. These results are fully consistent with the larger acidity of tungstates.

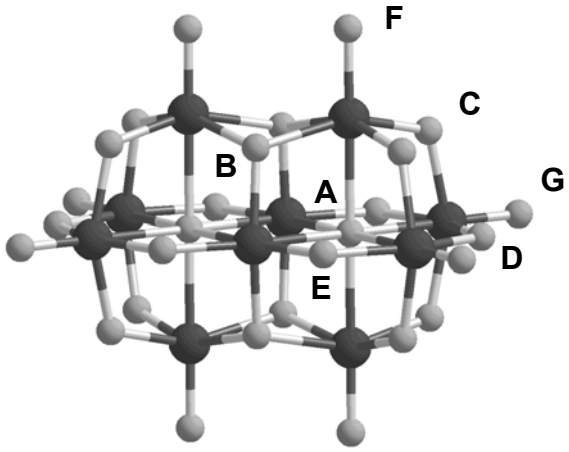

Figure 3.1. Spatial representation for $[V_{10}O_{28}]^{6-}$. The decavanadate anion has six distinct oxygen sites: one OV_3 (B), three OV_2 (C, D and E) and two OV (F, G).

The first attempt to classify the basicity of the various oxygen sites in a POM was reported by Bénard and co-workers at the beginning of the 1990's.[8] The decavanadate ion $[V_{10}O_{28}]^{6-}$ offered an excellent opportunity to compare the basicity of terminal (OV), double-bridging (OV_2) and triple-bridging (OV_3) oxygen sites in the same molecule. ^{17}O NMR spectroscopy for protonated and unprotonated species suggested that sites B and C (Figure 3.1) were the preferred protonation sites. This was confirmed by the crystallographic characterisation of the dimeric species $[H_3V_{10}O_{28}]^{6-}$. At that time, directly determining the protonation energy for a relatively large molecule like decavanadate was unaffordable and Bénard's group discussed the local basicity of a particular site by computing the distribution of Molecular Electrostatic Potentials. Electrophilic species tend to minimise their potential energy by approaching a minimum MESP value as much as possible. The EP distribution computed for the 26 external oxygen sites characterised 20 local minima, which were identified as probable protonation sites. The deepest ones were associated with the four triple-bridging oxygen sites B. Double bridging oxygens C and D were found at relative depths of 10 and 23 kcal mol^{-1}, respectively. According to this MESP distribution, the proton fixation preferentially takes place at the triple coordinated oxygens. The second preferred site is C and the protonation at O(term) is completely unexpected since the deepest minima in the vicinity of a terminal site appeared more than 55 kcal mol^{-1} above the minimum close to site B.

From *ab initio* calculations on fully optimised $M_2W_4O_{19}^{4-}$ (M = Nb and V) Lindqvist anions, Maestre *et al.*[9] determined the relative basicity of the external oxygens by means of three methods. On the one hand, protonation energies were computed for all oxo sites of the cluster and, on the other hand, atomic charges with Bader's population analysis[10] as well as the MESP distribution. The results agree with experimental observations since the deepest minimum of the electrostatic potential distribution is located near the OM_2 oxo site whereas terminal oxygens are the least basic.

Inclusion complexes and host-guest interactions

In a series of papers, Bénard's group analysed the electronic properties of inclusion complexes such as $RCN\subset(V_{10}O_{32})^{4-}$ and electronically inverse systems in which negatively charged species are encapsulated into negatively charged anions. These studies[11-12] have recently been reviewed at

length.[13] Figure 3.2 shows an inclusion complex characterised by the penetration of a nitrile in the hemisphere of a dodecavanadate anion.[14] For the acetonitrile complex, the experimental distance between the nitrile nitrogen and the plane that contains the four vanadium atoms at the bottom of the POM is 2.22 Å. The host-guest interaction between the two subunits remains in solution. The HF stabilisation energies for three R–CN guest molecules (R = H, CH_3 and C_6H_5) were found to have similar energies ranging from –12.8 to –14.4 kcal mol^{-1}.

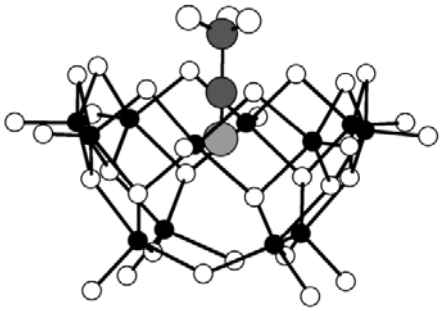

Figure 3.2. The inclusion complex $CH_3CN\subset[V_{12}O_{33}]^{4-}$. The black spheres represent metal atoms

A first analysis of the interaction between the host and guest molecules can be obtained from the MESP distributions of the two separate units. The MESP distribution for the $[V_{12}O_{32}]^{4-}$ cavity showed a saddle point that connects two regions of low potential, one in the bottom of the anion and the other more external. The upper minimum and the saddle point generate a dipolar moment that opposes that of the isolated guest nitrile. The weak stabilising interaction between N_2 and the host vanadate (–5 kcal mol^{-1}) emphasises the importance of a permanent dipole moment in the guest molecule. By superposing the MESP distributions for the host and guest subsystems, the potential minimum facing the N atom in C_6H_5CN coincided exactly with the saddle point in the host cavity. This means that the bonding between the two units follows a *lock* and *key* mechanism in which, as well as the coupling between the two opposing dipole moments, there is an electrostatic interaction between the nitrogen lone pair and the electrophilic region inside the cage. The absence of both a permanent dipole moment and

a lone pair makes C_2H_2 strongly repulsive toward the $[V_{12}O_{32}]^{4-}$ cavity, since its interaction energy was found to be +10.6 kcal mol^{-1}.

By decomposing the stabilisation energy using the CSOV method,[15] the bonding in the two observed inclusion complexes $RCN\subset(V_{10}O_{32})^{4-}$ (R = CH_3 and C_6H_5) and the model system $HCN\subset(V_{10}O_{32})^{4-}$ could be compared. For HCN and CH_3CN, the Steric term, which contains the Pauli repulsion and the Coulombic attraction, is dominated by the attractive interaction between host and guest units (–5.3 kcal mol^{-1} for R = H and –3.7 kcal mol^{-1} for R = CH_3). When the size of R increases, the Pauli repulsion between the substituent R and the anion increases and the Steric term becomes slightly positive (+1.8 kcal mol^{-1}). On the other hand, the guest polarisation and the charge transfer terms are larger for R = C_6H_5, which generally produces similar interaction energies for the three substituents.

Stabilising fields generated by counterions

Highly negative species like POMs only exist in condensed phases, where the external field generated by the solvent molecules or the counterions stabilise the anion. The instability of an *isolated* polyanion is manifested in the high energy of all its molecular orbitals.

Bénard[13] proposed the following procedure to incorporate the effect of the crystal field in quantum chemistry calculations of polyoxoanions:

1. Model the surrounding crystal by a set of point charges that can be determined from a Mulliken partition or from similar procedures.
2. Determine the electrostatic potential generated at the centre of the polyanion by the point charges contained in successive shells of ions until convergence.
3. Define a uniformly charged sphere of 20 Å in diameter, centred on the target anion and with a charge that is fitted to reproduce the potential obtained in the previous step.
4. Carry out a new quantum chemistry calculation with the presence of the charged sphere.

Using this procedure the stabilisation of guest anions inside negatively charged cages was analysed. Typical examples of these electronically inverse host-guest complexes are $Cl@[H_4V_{18}O_{42}]^{9-}$ and $Cl@[V_7O_{12}(O_3PR)_6]^{2-}$, clusters, in which a halogen is encapsulated by the

two anionic cages $[H_4V_{18}O_{42}]^{8-}$ and $[V_7O_{12}(O_3PR)_6]^-$. In agreement with the high negative charge of $[H_4V_{18}O_{42}]^{8-}$, the electrostatic potential at the centre of the cage is –0.57 a.u. This value means that the encapsulation of a negative charge has an associated electrostatic repulsion of +358 kcal mol^{-1}, which makes the encapsulation process of the *isolated* cage non-viable. For the non-protonated model complex $[V_{18}O_{42}]^{12-}$, the electrostatic potential is still more negative and reaches the value of –1 a. u. (–627 kcal mol^{-1}). In the less charged cage $[V_7O_{12}(O_3PR)_6]^-$, the potential at the centre of the cavity is positive (+0.06 a.u.) and therefore attractive towards a negative charge. These results for the electrostatic potential of the isolated cage can explain the formation of the $Cl@[V_7O_{12}(O_3PR)_6]^{2-}$ complex but do not allow us to rationalise the encapsulation of a halogen by a highly charged hollow cage like $[H_4V_{18}O_{42}]^{8-}$. Clearly, the crystal field is needed to achieve the stability of the encapsulation cluster. Bénard and co-workers estimated the lattice potential for $Cs_9(Cl@H_4V_{18}O_{42})$ and showed that it is *positive* at the centre of the cavity, thus overcoming the negative potential generated by the anionic host. An ample review of this subject can be found in reference 13.

One of the most important limitations when determining the lattice field is the disorder in many of the crystals that contain a polyoxoanion. The crystal structure for the salt $(Et_3H)_5(PMo_{12}O_{40}(VO)_2)$ was well solved and the potential due to the crystal could be estimated. The anion $[PMo_{12}O_{40}(VO)_2]^{5-}$ has 8 metal electrons and, unlike an oxidised cluster, this highly reduced system does not need a negative charge to complete the valence shell of oxo ligands. The $[PMo_{12}O_{40}(VO)_2]$ framework, with two VO units capping a Keggin structure, has a high tendency to be negatively charged, even at the gas phase. The total energy of the cluster exhibits a minimum when the net charge of the anion is –2 and –3. These values correspond to a number of 5 and 6 metal electrons over the metal ions, respectively. This means that the $Mo_{12}V_2$ cage has a high propensity to be negatively charged. However, the isolated cage cannot reproduce the optimal number of metal electrons in the cluster (8). The counterions generate a stabilising field (+0.393 a.u. on the central phosphorous) that increases the intrinsic tendency of the cluster to accept electrons: eight are accommodated on the d-metal orbitals.

Electronic structure of $[PMo_{12}O_{40}(VO)_2]^{5-}$

Maestre *et al*. performed DFT calculations on the Keggin-based bicapped $[PMo_{12}O_{40}(VO)_2]^{5-}$ anion.[16] This was synthesised by Hill and co-workers (Figure 3.3).[17] Such a cluster is 8 metallic electrons, and they are distributed between Mo centres and V capping units. Particularity, the two VO's are located at the positions. In this system, a competition between a singlet and a triplet state occurs.[18] The theoretical method utilised to obtain the correct ground state configuration was the Broken-Symmetry approach.[19] From experiments and DFT results it was concluded that each VO fragment has one unpaired electron, and that they are weakly ferromagnetically coupled. The singlet state was computed to be very close in energy, 0.77 kcal mol^{-1} above the ground state triplet state.

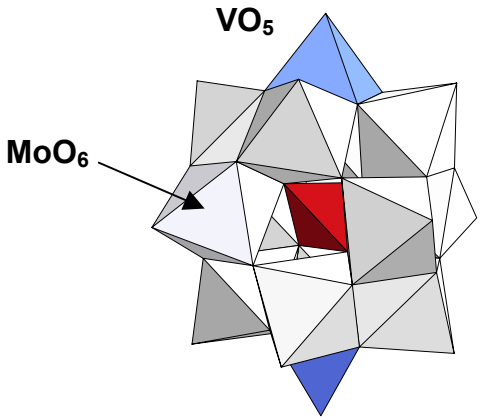

Figure 3.3. Polyhedral view of the $PMo_{12}(VO)_2$ anion, based on a bicapped Keggin framework.

3.3. More Recent Studies

Electronic structure and bonding in fully oxidised POMs

The most representative POM is the Keggin heteropolyanion (HPA), the formula of which is $[XM_{12}O_{40}]^{n-}$, where M is usually W^{6+} or Mo^{6+} and X, the *heteroatom*, is a main group or transition metal ion (P^{V}, Si^{IV}, Al^{III}, Ge^{IV}, Fe^{III}, Co^{II}, Co^{III}, Cu^{I}, Cu^{II}, etc.). The Keggin anion is made of an assembly

of twelve MO_6 octahedrons sharing their corners or edges with a central XO_4 tetrahedron (Figure 3.4). The metal–oxygen bonds in such a framework can be divided into three sets according to whether their oxygen atoms are tetrahedral (tetra), bridging (brid) or terminal (term). There is a fourth M–O bond type between the heteroatom and O(tetra). We will also use the notation O_m, where *m* indicates the number of ions bonded to the oxygen, throughout the text where it is convenient to do so. In the α-isomer, all metal centres are equivalent and the symmetry of the molecule is T_d. Marignac discovered a second isomer, today known as beta and with idealised C_{3v} symmetry. This differs from the α form in that there is a 60º rotation of one of the four edge-sharing M_3O_{13} triads. The common partial reduction of the *addenda* or *peripheral* M centres yields the intensely coloured "heteropoly blues". This term is normally used for reduced polyanions irrespective of their true colour.

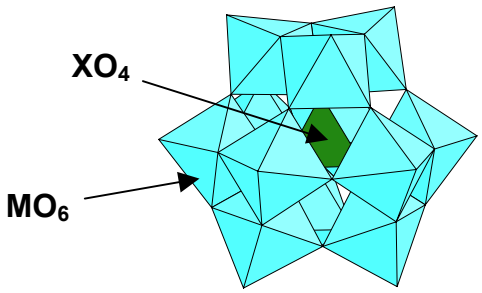

Figure 3.4. Polyhedral representation for an α-$[XM_{12}O_{40}]^{n-}$ Keggin anion. Blue octahedra are MO_6 units and the green tetrahedron contains the XO_4 unit.

Throughout this text we will use an abbreviated notation without oxygen atoms, charge or brackets, e.g., PW_{12} for $[PW_{12}O_{40}]^{3-}$ and $PW_{12}1e$ for $[PW_{12}O_{40}]^{4-}$, where *n*e identifies the number of electrons in the metal orbitals, or *blue* electrons. For clusters with paramagnetic ions, the explicit oxidation state of the heteroatom is given: $Co^{II}W_{12}1e$ represents a heteropolyblue with one delocalised electron among the twelve tungstens and the central cobalt ion in the oxidation state of +2.

In general, DFT calculations reproduce the geometry of HPAs very well. The exception is the M=O(term) bond lengths, which are systematically longer than the experimental ones. A systematic comparison of the theoretical and experimental geometries for several HPAs shows that

the deviation in the M=O(term) bond in Keggin and WD structures is on average 0.05 Å using the BP86 functional (Table 3.1). This discrepancy between the X-ray and the computed geometries is somewhat smaller (~0.03 Å) in isopolyanions such as $[M_6O_{19}]^{2-}$ (M = Mo and W),[20] and $[W_{10}O_{32}]^{4-}$ [21] using local functionals. For the highly charged Lindqvist anions $[Nb_6O_{19}]^{8-}$ and $[Ta_6O_{19}]^{8-}$, the experimental geometries are less well reproduced[20], probably because the crystal field effects are great and are not taken into account in these calculations.

Table 3.1. Comparison of theoretical (BP86/TZP) and X-ray (averaged values) distances (in Å) for a series of heteropolytungstates.

(a)		PW_{12}	SiW_{12}	AlW_{12}	$Co^{III}W_{12}$	$Co^{II}W_{12}$	$Fe^{III}W_{12}$
$X–O_n$	*DFT*	1.574	1.667	1.796	1.821	1.896	1.823
	Expt	1.53	1.64	1.74	1.79	1.90	1.82
X–W	*DFT*	3.579	3.532	3.526	3.565	3.547	3.567
	Expt	3.49	–	3.51	–	3.49	3.53
$W–O_1$	*DFT*	1.727	1.743	1.763	1.771	1.784	1.773
	Expt	1.69	1.71	1.71	1.71	1.71	1.72
$W–O_2$	*DFT*	1.932	1.916	1.930	1.943	1.946	1.944
		1.936	1.937	1.955	1.968	1.978	1.968
	Expt	1.90–1.91	–	1.90–1.96	1.85–1.97	1.88–1.99	1.88–1.96
$W–O_4$	*DFT*	2.424	2.325	2.242	2.265	2.203	2.263
	Expt	2.43	2.35	2.26	–	2.16	–

a) In $W–O_n$, *n* means the number of metal atoms coordinated to the oxygen atom.

In absence of paramagnetic ions, HPAs in general, and Keggin anions in particular, have a *simple* electronic structure in which the doubly occupied orbitals, formally delocalised over the oxo ligands, and the unoccupied set of d-metal orbitals are perfectly separated. In fully oxidised Keggin anions, the latter are symmetry-adapted d-metal orbitals with some antibonding participation of oxygen orbitals,

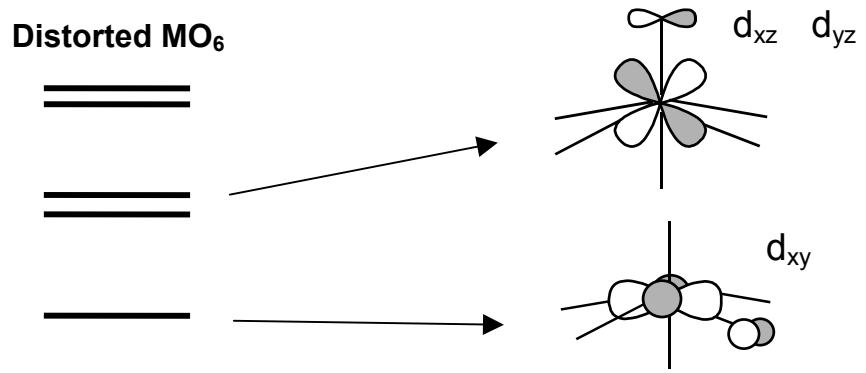

Due to the high oxidation state of metals in POMs, the t_{2g}-like orbitals are the most interesting in these clusters. Provided the MO_6 octahedra are distorted from the ideal O_h symmetry in Keggin anions, the d_{xy}, d_{xz} and d_{yz} orbitals are differently destabilised depending on how effective the antibonding interactions are with neighbouring p-oxygen orbitals. This overlap is more important between d_{xz} and d_{yz} with O(term) because the M=O bond lengths are shorter and the orientations are more favourable. Consequently, the LUMO in POMs are always symmetry-adapted combinations of d_{xy}-like orbitals. A 3D representation of one of the e symmetry components of both the degenerated HOMO and LUMO is given in Figure 3.5.

The energy gap between the occupied and the unoccupied band in Keggin anions without paramagnetic ions has been proven to be independent of X. Using the BP86 functional and a TZP-quality basis set for tungstates, Maestre *et al.* found a constant H-L gap of ~2.8 eV for different X.[22] At the same level of theory, this value decreases to 2 eV for molybdates. There is a direct relationship between the energy of the LUMO and the oxidising power of the POM. Therefore, the lesser energy of the lowest d-metal orbitals in molybdates means that they can generally be more easily reduced than tungstates to produce heteropoly blues. For example, it is well established that $SiMo_{12}$ and $GeMo_{12}$ are more powerful oxidising agents than the homologous tungstates by ~0.5 V. We frequently use the terms *band of unoccupied orbitals* and *oxo band*. It is worth noting though that these sets of orbitals do not form a band in the strict sense, since the orbitals are separated by discrete energies, at least for the relatively small clusters discussed here.

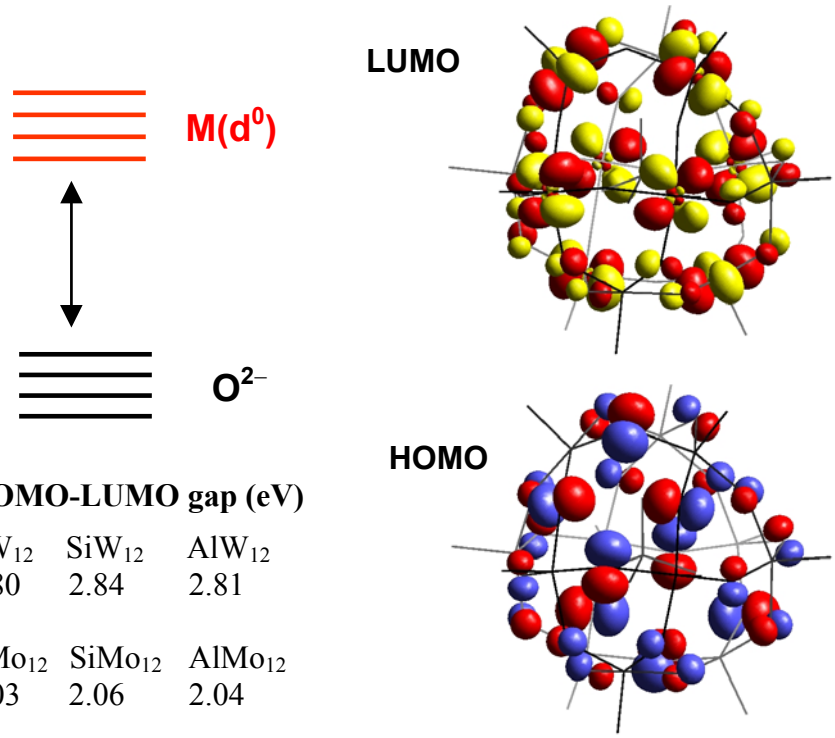

Figure 3.5. Molecular orbitals scheme for an α-Keggin anion. The separation between the M and O^{2-} bands represents the H-L gap, listed for a series of X and M. In $[SiW_{12}O_{40}]^{4-}$ the HOMO is composed in a 95% of p-oxygen orbitals whereas the LUMO has a 73% of d-metal orbitals. 3D-representations of one e component for each MO are showed.

Structure and bonding in single-addenda anions

Bridgeman and Cavigliasso described the nature of the occupied orbitals and bonding in several polyanions.[20-21,23-28] In a recent work, three sets of molecular energy levels were identified in $[M_6O_{19}]^{n-}$ Lindqvist structures: the low-lying orbitals basically composed of nonbonding combinations of s oxygen orbitals, the high-lying set composed of nonbonding combinations of p oxygen orbitals and an intermediate set that corresponds to M–O bonding interactions of essentially M(d)–O(p) character.[20] The gap between the s- and p-oxygen orbital sets is ~10 eV. An equivalent band structure was found for $[W_{10}O_{32}]^{4-}$ [21] and other isopolyanions. In $[TeM_6O_{24}]^{6-}$ and

$[PM_{12}O_{40}]^{3-}$ there is an additional level associated with the heteroatom that lies between the s and p oxo band (~7 eV above the s band). Delocalised σ and π bonds along the interpenetrating M–O closed loops are considered to be a structural-stability factor of a polyanion. For the $[W_{10}O_{32}]$ framework, for instance, two types of closed loops can be considered: the twelve-member W_6O_6 rings that are built along the *axial* direction and the eight-member W_4O_4 rings that lie in the *equatorial* planes.

A measure of the relative bonding capacity and strength of the distinct oxo ligands in an isopolyanion can be obtained through the formation process of a M_xO_y cluster as:

$$[M_xO_{y-1}]^{(n-2)-} + O^{2-} \rightarrow [M_xO_y]^{n-}$$

The average bonding energies (ΔE_B) for terminal, bridging and central oxygen atoms in Lindqvist structures showed that the loss of an O^{2-} ligand in $[M_6O_{19}]^{2-}$ to give the neutral cluster M_6O_{18} is highly endothermic (21–23 eV). These energies presumably would be different in solution since the O^{2-} anion is very unstable in the gas phase.

Table 3.2. Bond Lengths and Mayer Bond Order Indexes for $[M_6O_{19}]^{n-}$ Isopolyanions.[a)]

Molecule	M–O_6			M–O_2			M–O_1		
	LDA	*Expt.*	*B.O.*[a]	*LDA*	*Expt.*	*B.O.*[a]	*LDA*	*Expt.*	*B.O.*[a]
$[Mo_6O_{19}]^{2-}$	2.32	2.32	0.19	1.93	1.92	0.74	1.71	1.68	1.64
$[W_6O_{19}]^{2-}$	2.34	2.33	0.18	1.94	1.92	0.77	1.73	1.69	1.73
$[Nb_6O_{19}]^{8-}$	2.44	2.38	0.30	2.01	2.01	0.77	1.88	1.77	1.51
$[Ta_6O_{19}]^{8-}$	2.44	2.38	0.25	2.02	1.99	0.77	1.90	1.80	1.53

a) Mayer Bond order index.

It is interesting, however, to note the similarities in ΔE_B for the bridging and terminal sites, which show that bonding contributions for these two sites are similar even though they have different bond orders according to the Mayer bond order index[29] (Table 3.2). ΔE_B is somewhat smaller for the central oxygen. We can also see this trend in $[W_{10}O_{34}]^{4-}$, in which the

oxygen linked to five metal ions is again the site with the lowest bonding energy.[21] The connection between the values of the Mayer bond order index and the catalytic properties of a given anion, which are frequently associated with the loss of a terminal or a bridging oxygen, is not direct. One should take into account the effects of the solvent and the relaxation of the lacunary anion, which were not considered by Bridgeman.

Mixed-addenda clusters

Beyond the highly symmetric anions of formula $[XM_{12}O_{40}]^{n-}$, there are many clusters in which one or some $M^{n+}O_6$ octahedra have been formally replaced by another unit usually with a different metal centre like V^{5+}, Nb^{5+}, Ti^{4+}, etc. The distortion generated by this replacement is essentially limited to the region of substitution. Changes in the electronic structure are, however, much more important. The metal substitution modifies the energy and composition of the lowest unoccupied orbitals and, therefore, the redox properties of the molecule. Our group discussed this phenomenon for several mixed HPAs.[22] Although the ionisation energies of isolated metal ions computed suggest that the reduction of mixed-addenda molybdovanadates should occur at the molybdenum centres, the extra electron preferentially goes to a vanadium atom. Therefore, the reduced species $SiMo_{11}V^{IV}$ with one electron localised on the V centre is more stable than the heteropolyblue $SiMo_{11}V1e$ with one electron delocalised among the eleven Mo centres by 0.2 eV. The energy difference for the analogous tungstonvanadate $SiW_{11}V$ is 0.64 eV.[22]

Redox properties of clusters with nonequivalent metal sites

Extended-Hückel calculations[30] performed on the Wells–Dawson anion P_2W_{18} provided a qualitative understanding of the reduction process. It was found that the first metallic electron added to the cluster is belt-centred as experimental observations show. In addition, it was discussed the effect of addenda substitution in the WD framework. The localisation of the LUMO, the orbital directly involved in the first reduction, governs the distribution of the metal electrons.

As in WD structures, the metal atoms in the decatungstate anion $[W_{10}O_{32}]^{4-}$ can also be classified as *axial* and *equatorial* centres (see Figure 3.8). BP, BP86 and B3LYP calculations predict that the LUMO in

$[W_{10}O_{32}]^{4-}$ is an orbital of a_{1u} symmetry mainly delocalised over the equatorial centres.[21] Figure 3.6 shows orbital energies for the four lowest unoccupied orbitals and a plot of the LUMO in $[W_{10}O_{32}]^{4-}$. As expected from the composition of the LUMO, the ground states for the reduced species $[W_{10}O_{32}]^{5-}$ and $[W_{10}O_{32}]^{6-}$ are a doublet and a singlet, respectively, with the additional electrons delocalised among the equatorial sites. The diamagnetism predicted by the calculations for $[W_{10}O_{32}]^{6-}$ fully agrees with the experimental evidence. For the monoreduced species, the reduction at the axial centres (configuration $7b_{1u}^{1}$) was estimated to require ~1eV more than in the equatorial sites. By means of the energy decomposition scheme in terms of electrostatic interaction, Pauli repulsion and orbital mixing, Bridgeman *et al.* showed that the equatorial-reduced states are favoured by orbital mixing and to some extent by electrostatic factors. Otherwise, the states that involve the addition of one electron to the most distant axial sites have a smaller Pauli repulsion. In other words, as Borshch suggested from Extended Hückel calculations,[31] the gain in energy due to delocalisation over the equatorial sites exceeds the loss associated with the larger electronic repulsive effects and is the factor that determines the reduction site.

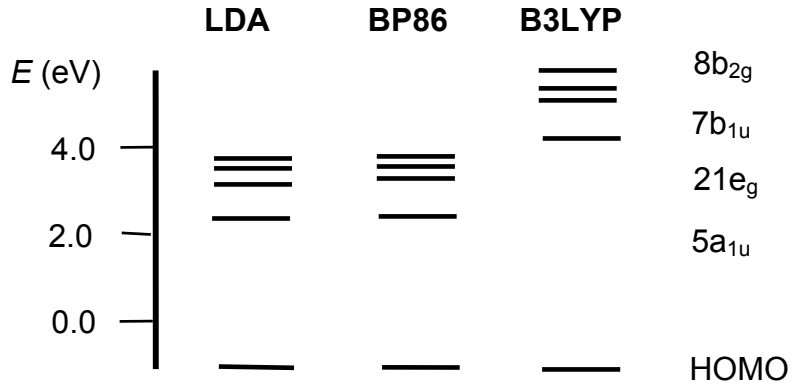

Figure 3.6. Frontier orbital diagram for $[W_{10}O_{32}]^{4-}$ computed with three functionals.

Heteropolyanions with paramagnetic ions

Heteropolyanions may incorporate *central* or *peripheral* paramagnetic transition metal ions. The structure of a Keggin anion, with a paramagnetic ion such as Fe^{III} or Co^{II} occupying the centre of the cluster, is not unlike those in which the heteroatom is a main group element (Table 3.1). A direct consequence of the lack of deformation in the $M_{12}O_{36}$ cage is that the energy gap between the doubly occupied oxo band and the set of unoccupied tungsten orbitals is not modified by the paramagnetic ion in the central tetrahedron. The value of 2.7 eV for the ground state of $Co^{II}W_{12}$ is very similar to the energy gap reported for Keggin clusters with main group heteroatoms, AlW_{12}, SiW_{12} and PW_{12} (2.8 eV). The d-cobalt orbitals appear well separated from the oxo and tungsten band, except for the unoccupied β–t_2 orbital, which is inserted into the tungsten band (Figure 3.7). The spin densities of Table 3.2 confirmed the high localisation of the unpaired electrons in the central tetrahedron XO_4. For $Co^{II}W_{12}$, the spin density is strongly localised in the cobalt centre (+2.56 e) but contributes little to the tetrahedral oxygens (+0.066 e per centre). For two other ions such as Co^{III} and Fe^{III}, the delocalisation of the spin density is somewhat higher.

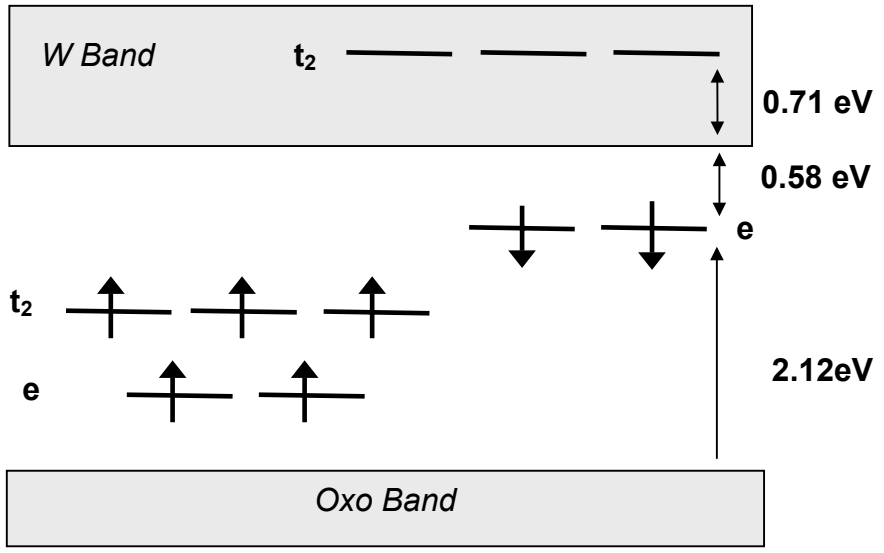

Figure 3.7. Frontier orbital region for the $[Co^{II}W_{12}O_{40}]^{6-}$ anion. The t_2 and e sets of orbitals correspond to the d orbitals of Co^{II}.

Table 3.2. Spin densities of several atoms in Keggin anions with paramagnetic ions in the central position.

	$Co^{III}W_{12}$	$Co^{II}W_{12}$	$Fe^{III}W_{12}$
Fe/Co	+2.867	+2.565	+4.003
W	–0.003	+0.002	–0.001
O_4	+0.226	+0.066	+0.193
O_2	+0.002	+0.001	+0.002
O_2'	+0.015	+0.008	+0.012
O_1	+0.006	+0.002	+0.006

It is well established that the first reduction of $Co^{III}W_{12}$ takes place at the cobalt ion and produces $Co^{II}W_{12}$, whereas the subsequent reduction produces the heteropolyblue $Co^{II}W_{12}1e$ instead of $Co^{I}W_{12}$. On the other hand, the reduction of $Fe^{III}W_{12}$ leads directly to the blue species $Fe^{III}W_{12}1e$. For the ground state of $[CoW_{12}O_{40}]^{6-}$, the promotion of 1e from the highest β Co orbital to the lowest W orbital requires ~1eV. This large amount of energy explains why the blue species $Co^{III}W_{12}1e$ is not the reduction product of $Co^{III}W_{12}$ because the additional electron goes to the cobalt orbital. The subsequent reduction, however, does not occur at the cobalt centre because the blue species $Co^{II}W_{12}1e$ is 0.78 eV more stable than $Co^{I}W_{12}$. This is a product that requires the addition of one electron to the $\beta–t_2$ orbital, which is 0.71 eV above the lowest unoccupied tungsten orbital.

The unrestricted DFT energies computed for an open-shell configuration represent an average of the individual multiplets associated with a given configuration. The energy of a particular multiplet can be formulated as the weighted sum of single determinant energies. With the aid of the STAGEN program for determining the symmetry coefficients for wave functions and energies,[32] Maestre *et al.* computed the multiplet splittings for several excited configurations of $[Co^{II}W_{12}O_{40}]^{6-}$.[33] For the excited $e^3t_2^4$ configuration there are two quadruplets of symmetries $T_2(F)$ and $T_1(F)$ that are at 7126 and 13711 cm^{-1} above the $^4A_2$ ground state, which is associated with the ground configuration $e^4t_2^3$. These energies are too large if we compare them with the assignments made for the permitted Co → Co transition $^4A_2 \rightarrow {}^4T_1$ (7830 cm^{-1}) and the forbidden transition $^4A_2$

$\rightarrow {}^4T_2$ (4600 cm^{-1}). There is strong agreement when a Jahn–Teller relaxation is permitted for the excited configurations. The states $^4T_1$ and $^4T_2$ in the T_d geometry split into the four states $^4B_2$, $^4E(2)$ and $^4A_2$ in the D_{2d} geometry. The lowest state of symmetry B_2 appears at 5275 cm^{-1}, a value that agrees fairly well with the energy expected for the forbidden transition $^4A_2 \rightarrow {}^4T_2$. The energies of the next excited states range between 7700 and 11000 cm^{-1}. These values agree well with the presence of an intense, broad band in the near-infrared region (7000–9000 cm^{-1}) in the electronic spectrum of $[Co^{II}W_{12}O_{40}]^{6-}$. Superposed to the Co $\rightarrow$ Co transitions are charge-transfer transitions from Co to W.

Substituting addenda metal atoms by paramagnetic ions provides highly interesting clusters. Derivatives containing Mo and Fe are one example. The closeness of the redox potentials for Mo^{VI}/Mo^{V} and Fe^{III}/Fe^{II} in oxides allows the equilibrium

$$Fe^{II} + Mo^{VI} \rightarrow Fe^{III} + Mo^{V}$$

when both ions are in octahedral sites. Duclusaud and Borshch studied this process[34] in the Keggin framework through a model cluster including only the region of Fe and two neighbouring Mo atoms. Two minima that differ by less than 1 kcal mol^{-1} were found at the B3LYP level, corresponding to the one-electron-transfer between Fe and Mo. Two configurations were computed: case A is the situation in which all metal electrons are at the iron centre with a high-spin configuration, $t_2{}^4e^2$, and with one β-electron in the orbital. Case B is the configuration in which this β-electron has been transferred to a molybdenum orbital. The only noticeable difference between the geometries of A and B is the coordination sphere around Fe, which is more contracted in B. The small energy difference between the two localisation patterns and the probable absence of an energy barrier between them suggest fast electronic hopping between the states. This would agree with the interpretation of the Mössbauer spectra for this sort of system.[34] A similar model was used to describe the electron transfer between a Keggin unit and an Fe counterion.[35]

Magnetic properties of reduced polyoxoanions

Coupling between blue electrons and paramagnetic ions. POMs are versatile building blocks for constructing molecular magnetic materials.

Many POM-based materials present the coexistence of localised and delocalised magnetic electrons. An example of this situation is given in the heteropolyblue $Fe^{III}W_{12}1e$, in which the five unpaired central electrons are *antiferromagnetically* coupled with the external electron delocalised over the Ws. According to this magnetic behaviour, the low-spin state, determined by the Broken-Symmetry approach, was computed to be 196 cm^{-1} more stable than the high-spin state computed at the unrestricted level. For $Co^{II}W_{12}1e$, the coupling between the external and the three internal cobalt electrons is slightly *ferromagnetic*, with an energy difference between the two spin states of only 21 cm^{-1}.[22]

Duclusaud *et al.*[36] evaluated the magnetism modulated by the nitrosyl derivative of the decamolybdate ion, $[Mo_{10}O_{25}(OMe)_6(NO)]^-$, is affected by the position of the six metoxi ligands. The structure of this anion is related to that of $[Mo_{10}O_{34}]^{4-}$ (Figure 3.8) and may be viewed as a $Mo_{10}O_{34}$ framework in which one terminal oxygen is replaced by a NO group and six bridging oxygens are replaced by six metoxi groups. By modelling the CH_3

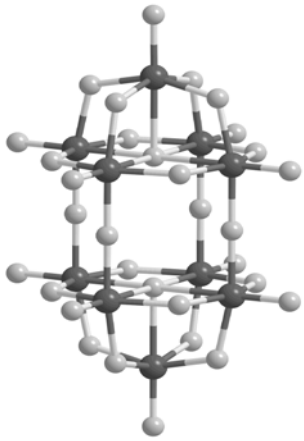

Figure 3.8. Structure of the $[Mo_{10}O_{34}]^{4-}$ anion. One of the axial terminal oxygens was replaced by a NO group, whereas several other oxo positions were substituted to study the changes produced in the MO structure (see text).

groups with H atoms, five positional isomers were studied. As in $[W_{10}O_{34}]^{4-}$, the LUMO for the fully oxidised parent of **I** ($[Mo_{10}O_{25}(OMe)_6(NO)]^+$) is an orbital delocalised over the eight equatorial

Mo ions, and well separated from the next unoccupied level. Consequently, the two additional electrons are accommodated in the LUMO, which gives rise to a diamagnetic ground state for $[Mo_{10}O_{25}(OMe)_6(NO)]^-$. We could modify the diamagnetism of this anion if we could reduce the H-L gap and get an open-shell state (triplet or singlet competitive with the closed-shell configuration). Since the HOMO in $[Mo_{10}O_{25}(OMe)_6(NO)]^-$ is localised on the eight equatorial molybdenum ions, we expect the protonation in the bridging oxygens of the equatorial planes or between the equatorial planes to alter the energy of the HOMO and its separation with respect to the LUMO. See reference 6 for more information. To sum up, Duclusaud and Borshch have proven that the magnetic properties of a reduced cluster can be conveniently tuned by controlling the position of a substituent in POMs.

Ab initio determination of electron-transfer parameters in reduced Keggin anions. Experimentally, it is well established that when Keggin anions contain an even number of delocalised electrons the compound is diamagnetic. Initially, this phenomenon was attributed to a strong antiferromagnetic coupling via a superexchange mechanism.[37] It was later shown through model calculations that electron delocalisation and electron repulsion can stabilise the diamagnetic singlet.[38] Coronado and co-workers recently reported very accurate *ab initio* calculations to evaluate electron-transfer parameters in reduced Keggin anions.[39] Provided that the transfer (hopping) effective integrals are essentially local parameters, fragments can properly model the Keggin framework. These authors used 4W- and 2W-ion fragments (Figure 3.9) to estimate transfer integrals in the one-electron-reduced cluster. Taking into account that the unpaired electrons are delocalised over d_{xy}-like orbitals of W ions, the following four doublets can be defined for the one-electron-reduced 4W-ion fragment,

$$\psi_1 = \frac{d_1 + d_2 + d_3 + d_4}{2},\ \psi_2 = \frac{d_1 - d_2 - d_3 + d_4}{2}$$

$$\psi_3 = \frac{d_1 + d_2 - d_3 - d_4}{2},\ \psi_4 = \frac{d_1 - d_2 + d_3 - d_4}{2}$$

where d_i are the Slater determinants constructed when the extra electron is on the corresponding W_i ions. In this context, the transfer parameters t

(hopping between corner-sharing WO_6 octahedra) and *t'* (hopping between edge-sharing WO_6 octahedra) are then written as:

$$t = \langle d_1 | H | d_4 \rangle \quad t' = \langle d_1 | H | d_2 \rangle$$

These integrals are related to the doublet energies $E_1 - E_4$ by the equations,

$$E_4 - E_1 = -2t - 2t', \quad E_3 - E_2 = -2t + 2t'$$

By precisely determining the E_i energies the values obtained for *t* and *t'* are also very accurate. Contrary to what is commonly accepted, the electron transfer between edge-sharing and corner-sharing WO_6 octahedra was very similar for all methods and fragments used. For the largest fragment, the best calculation was performed at the CASPT2 level, giving a value of –428 meV for *t* and –470 meV for *t'*. The computed values at the same level of accuracy did not differ very much when the smallest 2W-based fragments of Figure 3.9-d (–445 and –490 meV, respectively) were used.

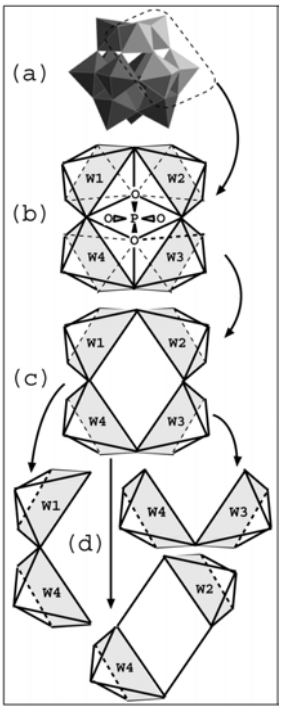

Figure 3.9. (a) Polyhedral representation for a Keggin anion. (b)–(d) Fragments used to compute transfer (hopping) integrals. Reproduced from ref. 39.

For these smaller clusters, t and t' integrals were also calculated with the variational DDCI method, leading to t = –467 meV and t' = –507 meV. When the latter values were introduced into an extended Hubbard Hamiltonian[39], the singlet state for a two-electron-reduced Keggin anion was estimated to be 280 meV more stable than the lowest triplet state. This large energy gap clearly explains the diamagnetism of the two-electron-reduced Keggin anions.

Localisation/delocalisation of the metal electrons in mixed-addenda POMs

Most POMs comprising metal ions in a high oxidation state can be easily reduced without making significant structural changes. It is difficult to unequivocally characterise the number and nature of the reduced centres in a partly reduced cluster and today this is still a matter of debate. Electrochemical reductions and EPR spectroscopy have usually been used to determine the localisation, or delocalisation, of the metal electrons in reduced HPAs. The intense blue colour in reduced POMs is considered to indicate an important delocalisation of the metal electrons.

As we have mentioned above, the monoreduction of the mixed $SiVW_{11}$ anion yields the brown species $SiV^{IV}W_{11}$, not the heteropoly blue, $SiVW_{11}1e$. The first two electrochemical reductions in $SiMoV_2W_9$ and the first three electrochemical reductions in SiV_3W_9 were attributed to $V^V \rightarrow V^{IV}$ steps.[40] Through empirical valence sum calculations based on the X-ray structure of the highly reduced bicapped Keggin complex $[PMo_{12}O_{40}(VO)_2]^{5-}$, two of the eight d electrons were assigned to the two V centres and the other six electrons were considered to be delocalised among the other 12 Mo centres.[41] This distribution was fully confirmed by DFT calculations, which showed that the ground state was a triplet with two V^{IV} ions.[42] The alternative configuration, corresponding to an equipartition of the eight electrons between vanadium and molybdenum centres, was less stable by 1.41 eV. Xu *et al*. synthesised the related tetracapped cluster $[Mo_8V_8O_{40}(PO_4)]^{5-}$ as an anion with eight V^{IV} centres with the other two d electrons delocalised over the eight Mo atoms.[43] When then number of vanadium ions increases, the hypothesis that before accommodating any electron in a Mo orbital all vanadium centres should have at least one electron does not seem to be satisfied. Preliminary calculations carried out by our group on $[Mo_8V_8O_{40}(PO_4)]^{5-}$ indicate that the configuration with eight electrons on the 8 V centres and the two remaining electrons on the 8

Mo atoms is ~2 eV more unstable than the more equilibrated repartition of the electrons i.e. six electrons over the V centres and the other four electrons over the Mo centres.

Using DFT/BP86 calculations, Rohmer and Bénard discussed the nature of the M–M bond in the two-reduced oxothio clusters γ-$[SiW_{10}M_2S_2O_{38}]^{6-}$ (M = Mo, W) recently synthesised by Cadot and Sécheresse.[44] The X-ray characterisation of these structures revealed short M^V–M^V distances (2.832 Å for M = Mo and 2.815 Å for M = W). These values clearly indicate that Mo–Mo and W–W are single bonds. The oxoanions γ-$[SiW_{10}Mo_2O_{40}]^{6-}$ and γ-$[SiW_{12}O_{40}]^{6-}$ were also synthesised but could not be characterised crystallographically. For the four anions a first minimum with a short M–M separation was found. The computed M–M separations in the oxothio anions, 2.998 Å for M = Mo and 2.872 Å for M = W, were somewhat longer than the distances observed but these structures maintained the presence of a metal-metal coupling. The corresponding metal–metal distances for the oxo anions were 2.653 and 2.569 Å. All the complexes have similar electronic structures, an occupied valence O/S band that is well separated from the empty d-Mo/W band and an isolated HOMO localised on the $M_2X_2O_2$ fragment that is typical of a σ_{M-M} bond:

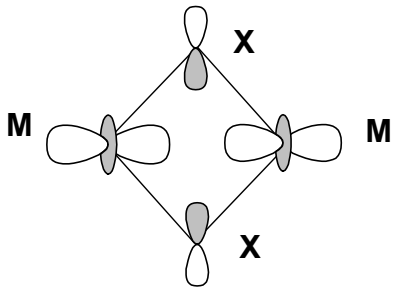

A new minimum characterised by a long M–M distance (>3 Å for X = O and >3.7 Å for X = S) and with the two electrons delocalised over the γ-Keggin tungstate was reported. Except for γ-$[SiW_{12}O_{40}]^{6-}$, the most stable conformation is the one with the short metal-metal distance, with energies ranging from 10.2 to 23.8 kcal mol^{-1}. In the unsubstituted tungstate, the delocalised state is lower in energy by 2.9 kcal mol^{-1} This seems to be consistent with the blue colour of the anion in solution. The other three anions are red or red-brown. The localisation/delocalisation of the two metal

electrons in the γ-$[SiW_{10}M_2X_2O_{38}]^{6-}$ clusters therefore depends on the difference between the electrophilic characters of the Keggin core, γ-$[SiW_{10}O_{36}]^{n-}$, and the flexible dimetallic fragment, $M_2X_2O_2$.[44]

Proton affinity of polyoxoanions

Amoureux and co-workers[45] used BP86 functional and a TZP-quality basis set to study the basicity of single-addenda PM_{12} anions (M = Mo, W). As expected, the protonation in the bridging oxygen sites was preferred. Protonations at terminal (O_1) oxygen were less favoured by 11.5 and 18.4 kcal mol^{-1} for PMo_{12} and PW_{12}, respectively. These values were compared with Rotational Echo Double Resonance (REDOR) NMR data, which detected the protons in $H_3PMo_{12}O_{40}$ and $H_3PW_{12}O_{40}$ at a distance of 5.20±0.20 Å and 5.70±0.20 Å from the central phosphorus, respectively. Both experimental values were rather larger, especially the latter. This seems only consistent with a protonation at a terminal site in H_3PW_{12}. For the first time, the general assumption that the protonation at a terminal oxygen site is only competitive in systems containing Nb, Ti or Cr was called into question. In our opinion, these results are very important because, if confirmed in other systems, they may indicate that solvent and counterions need to be considered to find the local active sites in a POM.

Slightly out of the scope of molecules presented here, let us comment a similar work conducted on a novel tin nanocluster, $[(CH_3Sn)_{12}O_{14}(OH)_6]^{2+}$. Wavefunction-based and DFT calculations[46] were aimed at studying the nature of the interactions between ―anionic and neutral― nucleophilic species and the cited cluster. Molecular electrostatic potentials were computed to confirm the experimental observations on the regioselectivity of the nucleophiles towards the tin cation. The basicity of the oxygen sites of the cluster was investigated by means of the protonation energy and the atomic charge. The hardness/softness principle applied to the system did not probed to describe correctly all the nucleophile-cluster interactions, thus showing that electrostatic considerations and hydrogen bonding are much more important.

Vibrational frequencies in Lindqvist and Keggin anions

The theoretical determination of vibrational frequencies for large molecules is still a non-standard task. In the case of Keggin anions, the calculation of

the second derivatives of the energy is extremely computational demanding despite their tetrahedral symmetry. In a significant study, Bridgeman computed, classified and compared the vibrational frequencies for the series of Keggin anions $[XMo_{12}O_{40}]^{n-}$, X = P^{III}, As^{III}, Si^{IV}, Ge^{IV}, Al^{V} and Ga^{V} and $[PW_{12}O_{40}]^{3-}$ using the B3LYP hybrid functional.[47] We will not describe here the 153 normal modes of vibration of an α-Keggin anion but we should point out that the B3LYP functional with augmented LANL2DZ basis sets reproduces the experimental spectrum of Keggin anions very well. The discrepancy between the calculated and the observed spectra does not exceed a few cm^{-1} for most vibrational modes. For $[PW_{12}O_{40}]^{3-}$, the largest deviation of 71 cm^{-1} takes place in a vibrational mode assigned as a combined stretching and bending Mo–O–Mo mode. Previously, the same group compared the vibrational spectra of various Lindqvist anions at several computational levels. Although DF methods reproduce the vibrational spectral of $[M_6O_{19}]^{n-}$ clusters quite well, the HF method performs very poorly.[48] The fitting between experimental and theoretical spectra was best at the LDA level with the TZP/ZORA approach (triple-ζ Slater basis set with the ZORA method). In comparison, the LDA and B3LYP functionals with GTO basis provide less accurate results. The results with BP86 and BLYP are significantly poorer.[48]

References and Notes

[1] Davidson, E. R. *Chem. Rev.* **2000**, *100*, 351.

[2] Fonseca Guerra, C.; Snijders, J. G.; Te Velde, G.; Baerends, E. J. *Theor. Chem. Acc.* **1998**, *99*, 391 and references therein.

[3] Jansen, S. A.; Singh, D. J.; Wang, S-H. *Chem. Mater*. **1994**, *6*, 146.

[4] Wang, S-H.; Jansen, S. A. *Chem. Mater*. **1994**, *6*, 2130.

[5] Wang, S-H.; Jansen, S. A.; Singh, D. J. *J. Cat*. **1995**, *154*, 137.

[6] Poblet, J. M.; López, X.; Bo, C. *Chem. Soc. Rev.* **2003**, 32, 297.

[7] Bardin, B.; Bordawekar, S. V.; Neurock, M.; Davis, R. J. *J. Phys. Chem. A*. **1998**, *102*, 10817. See also Bardin, B.; Davis, R. J.; Neurock, M. *J. Phys. Chem. B*. **2000**, *104*, 3556.

[8] Kempf, J. Y.; Rohmer, M.-M.; Poblet, J. M.; Bo, C.; Bénard, M. *J. Am. Chem. Soc.* **1992**, *114,* 1136.

[9] Maestre, J. M.; Sarasa, J. P.; Bo, C.; Poblet, J. M. *Inorg. Chem*. **1998**, *37*, 3071.

[10] Bader, R. F. W. *Atoms in Molecules. A Quantum Theory*. Clarendon Press, Oxford, **1990**. Bader, R. F. W. *Chem. Rev*. **1992**, *91*, 893.

[11] Rohmer, M.-M.; Bénard, M. *J. Am. Chem. Soc.* **1994**, *116,* 6959.

[12] Rohmer, M.-M.; Devémy, J.; Wiest, R.; Bénard, M. *J. Am. Chem. Soc.* **1996**, *118,* 13007.

[13] Rohmer, M.-M.; Bénard, M.; Blaudeau, J.-P.; Maestre, J. M.; Poblet, J. M. *Coord. Chem. Rev.* **1998**, *178–180*, 1019.

[14] Day, V. W.; Klemperer, W. G.; Yaghui, O. M. *J. Am. Chem. Soc.* **1989**, *111*, 5959.

[15] Bagus, P. S.; Bauschlicher, C. W.; Nelin, C. J.; Laskowski, B. C. *J. Chem. Phys.* **1984**, *81*, 3594.

[16] Maestre, J. M.; Poblet, J. M.; Bo, C.; Casañ-Pastor, N.; Gómez-Romero, P. *Inorg. Chem.* **1998**, *37*, 3444.

[17] Chen, Q.; Hill, C. L. *Inorg. Chem.* **1996**, *35*, 2403.

[18] Borshch, S. A.; Bigot, B. *Chem. Phys. Lett*. **1993**, *212*, 398.

[19] Noodleman, L. J. *Chem. Phys*. **1981**, *74*, 5737. Noodleman, L.; Davidson, E: R. *Chem. Phys*. **1986**, *109*, 131. Noodleman, L.; Case, D. A. *Adv. Inorg. Chem*. **1992**, *38*, 423. Noodleman, L.; Pen, C. Y.; Case, D. A. Mouesca, J. M. *Coord. Chem. R*ev. **1995**, *144*, 199.

[20] Bridgeman, A.; Cavigliasso, G. *Inorg. Chem.* **2002**, *41*, 1761.

[21] Bridgeman, A.; Cavigliasso, G. *J. Phys. Chem. A*. **2002**, *106*, 6114.

[22] Maestre, J. M.; López, X.; Bo, C.; Poblet, J. M.; Casañ-Pastor, N. *J. Am. Chem. Soc.* **2001**, *123*, 3749.

[23] Bridgeman, A.; Cavigliasso, G. *Polyhedron.* **2001**, *20*, 3101.

[24] Bridgeman, A.; Cavigliasso, G. *J. Phys. Chem. A*. **2001**, *105*, 7111.

[25] Bridgeman, A.; Cavigliasso, G. *J. Chem. Soc., Dalton Trans.* **2001**, 3556.

[26] Bridgeman, A.; Cavigliasso, G. *J. Chem. Soc., Dalton Trans.* **2002**, 2244.

[27] Bridgeman, A. *J. Phys. Chem. A*. **2002**, *106*, 12151.

[28] Bridgeman, A.; Cavigliasso, G. submitted for publication.

[29] Mayer, I. *Chem. Phys. Lett*. **1983**, *97*, 270. Mayer, I. *Int. J. Quant. Chem*. **1984**, *26*, 151.

[30] Keita, B.; Jean, Y.; Levy, B.; Nadjo, L.; Contant, R. *New J. Chem*. **2002**, 1314.

[31] Borshch, S. A. *Inorg. Chem.* **1998**, *37*, 3116.

[32] Daul, C. *Int. J. Quantum Chem*. **1994**, *52*, 867.

[33] Maestre, J. M.; López, X.; Bo, C.; Daul, C.; Poblet, J. M. *Inorg. Chem.* **2002**, *41*, 1883.

[34] Duclusaud, H.; Borshch, S. A. *Inorg. Chem.* **1999**, *38*, 3491.

[35] Borshch, S. A.; Duclusaud, H.; Millet, J. M. *Appl. Cat. A: General*. **2000**, *200*, 103.

[36] H. Duclusaud, S. A. Borshch, *J. Am. Chem. Soc.* **2001**, *123*, 2825.

[37] Casañ-Pastor, N.; Baker, L. C. W. *J. Am. Chem. Soc.* **1992**, *114*, 10384 and references therein.

[38] Borrás-Almenar, J. J.; Clemente-Juan, J. M.; Coronado, E.; Tsukerblat, B. S. *Chem. Phys.* **1995**, *195*, 1.

[39] Suaud, N.; Gaita-Ariño, A.; Clemente-Juan, J. M.; Sánchez-Marín, J.; Coronado, E. *J. Am. Chem. Soc.* **2002**, *124*, 15134.

[40] Cadot, E.; Fournier, M.; Tézé, A.; Hervé, G. *Inorg. Chem.* **1996**, *35*, 282.

[41] Chen, Q.; Hill, C. L. *Inorg. Chem.* **1996**, *35*, 2403.

[42] Maestre, J. M.; Poblet, J. M.; Bo, C.; Casañ-Pator, N.; Gómez-Romero, P. *Inorg. Chem.* **1998**, *37*, 3444.

[43] Xu, Y.; Zhu, H-G.; Cai, H.; You, X.-Z. *Chem. Commun.* **1999**, 787.

[44] Rohmer, M.-M.; Bénard, M.; Cadot, E.; Secheresse, F. *Polyoxometalate Chemistry*. Pope, M. T.; Müller, A., eds., pp. 117–133. Kluwer Academic Publishers. The Netherlands, **2001**.

[45] Ganapathy, S.; Fournier, M.; Paul, J. F.; Delevoye, L.; Guelton, M.; Amoureux, J. P. *J. Am. Chem. Soc.* **2002**, *124*, 7821.

[46] Vivas-Reyes, R.; De Proft, F.; Geerlings, P.; Biesemans, M.; Willem, R.; Ribot, F.; Sanchez, C. *New J. Chem*. **2002**, *9*, 1093.

[47] Bridgeman, A. *Chem. Phys.* **2003**, *287*, 55.

[48] Bridgeman, A.; Cavigliasso, G. *Chem. Phys.* **2002**, *279*, 143.